Boundary migration during recrystallization: experimental observations

Zhang, Yubin; Juul Jensen, Dorte

Published in:
I O P Conference Series: Materials Science and Engineering

Link to article, DOI:
10.1088/1757-899X/89/1/012015

Publication date:
2015

Document Version
Publisher's PDF, also known as Version of record

Boundary migration during recrystallization: experimental observations

2015 IOP Conf. Ser.: Mater. Sci. Eng. 89 012015

(http://iopscience.iop.org/1757-899X/89/1/012015)

Boundary migration during recrystallization: experimental observations

Y B Zhang, D Juul Jensen

Section for Materials Science and Advanced Characterization, Department of Wind Energy, Technical University of Denmark, Risø Campus, Roskilde 4000, Denmark

E-mail: yubz@dtu.dk

Abstract. Quantitative analysis of boundary migration during recrystallization is a key task to understand the recrystallization process and to improve recrystallization models. In the last 25-30 years, quantification of boundary migration has mostly been conducted in term of average growth rates in many materials. This type of analysis has largely been based on the assumption that all or groups of recrystallizing grains grow in the same uniform manner, therefore the results represent average growth behaviors on a *macro* scale. Recently, significant efforts have been made to quantify the boundary migration during recrystallization on *local* grain scales, using different advanced experimental characterization and computer simulation techniques. This paper aims at summarizing these recent achievements with focus on the potentials of the various advanced experimental characterization techniques. Suggestions for new experimental and simulation work important for advancing the current understanding of local boundary migration are finally discussed.

1. Introduction

During recrystallization, nearly perfect, dislocation-free nuclei develop at preferential sites in the deformed microstructure and grow by boundary migration through the deformed matrix, until the whole deformed matrix is replaced by recrystallized grains. The boundary migration rate, v, is generally expressed as:

$$v = MF \tag{1}$$

where M is the boundary mobility and F is the driving force for migration. For recrystallization F is typically considered as the energy stored in the deformed matrix [1]. Experimentally, this equation has been frequently validated for boundary migration during the grain growth process (typically occurring after recrystallization is complete) [2], but more rarely for boundary migration during recrystallization. The few recrystallization studies quantifying equation (1) have been conducted by static stereological 2D characterizations, and the analysis is thus only valid for the average behavior of groups of grains (e.g. [3]). Also along the same lines, many studies of recrystallization have focused on recrystallization kinetics and estimated average boundary migration rates using e.g. the Cahn-Hagel [4] and the extended Cahn-Hagel method [5] based on stereological analysis or using maximum grain sizes [6].

In the last 25-30 years, lots of works on characterization of deformation microstructures have shown that deformation microstructures in most metals are highly heterogeneous (e.g. [7]) and depend on the crystallographic orientations of the deformed grains (e.g. [8]). At the same time, several new

experimental characterization techniques have been developed, such as in-situ measurements using electron backscattered diffraction (EBSD) techniques (e.g. [9]) and 3D X-ray diffraction (3DXRD) techniques (e.g. [10]), which allow detailed quantification of boundary migration and in some cases of the deformed microstructure in front of the migrating boundary on a *local* grain scale in 2D or 3D. These techniques have been used to study recrystallizing boundaries and their migration into different deformed grains on the local scale. The results have shown that locally the migration is much more complex than hitherto assumed: the migration of individual boundary segments occurs in a jerky stop-go fashion, and fairly large protrusions and retrusions often form and evolve on many boundaries (e.g. [11]). It has therefore been suggested that the local heterogeneities in the deformed microstructures have to be taken into account for a comprehensive understanding of the local recrystallization boundary migration [12].

The aim of this paper is to summarize experimental achievements in this relatively new research field of local recrystallization boundary migrations. The main focus will be on the quantification of local protrusions/retrusions and of their effects on the boundary migration as well as on the effects of the local deformed microstructures in front of the recrystallizing boundaries. The paper is organized in sections according to the experimental techniques used for the studies: i.e. 2D (x, y), 3D (x, y, z) and (x, y, t) as well as 4D (x, y, z, t). Potentials of the experimental techniques and suggestions for future work will be discussed at the end.

2. 2D (x, y) static characterizations

Partially recrystallized microstructures can be revealed by many microscopical techniques such as optical microscopy (OM), electron channeling contrast (ECC), electron backscattered diffraction (EBSD), and transmission electron microscopy (TEM). Among these techniques, OM is certainly the easiest to use, and used to play an important role in the early days for recrystallization studies (e.g. [13]). Nowadays, due to the wide availability of scanning electron microscopes (SEMs), OM is generally only used as a simple tool to get a quick characterization of the recrystallization state on a macro scale.

The ECC and EBSD within SEMs are now more commonly used to visualize recrystallizing structures. The ECC techniques can easily provide spatial resolution of ~1 nm [14], whereas EBSD can typically provide a spatial resolution of 20-30 nm. This lower resolution is because of the large interaction volume of the electron beam and sample surface at a high tilting angle [15]. EBSD techniques however provide unique possibilities for mapping microstructures with full information of crystallographic orientations (angular resolution of 1.5-2°), which allows quantitative analysis of local microstructures and textures of both the deformed matrix and the recrystallized grains [9]. EBSD is therefore nowadays the most frequently used technique for recrystallization studies, e.g. in the latest recrystallization conference proceeding ~76% of the papers on experimental studies of recrystallization were based on measurements conducted using EBSD techniques [16].

TEM (incl. high voltage TEM) techniques can characterize microstructures with the highest spatial resolution down to the atomic level. Free dislocations and the dislocation content in dislocation boundaries (e.g. [17]) can be characterized with TEM but not with any of the above mentioned techniques. Before the appearance and commercializing of the EBSD techniques, TEM was the most important tool for detailed recrystallization studies (e.g. [18]). One of the drawbacks with TEM is that it is not so easy to determine crystallographic orientations over large area as with EBSD. Even using semi-automatic methods [19] by which the crystallographic orientations can be determined at a reasonable speed, the efficiency can still not be comparable with that of EBSD. A relatively high angular resolution (~0.5°) can, however, be obtained. Besides that, the sample preparation is difficult for TEM and to prepare a good large TEM sample for statistical analysis is even more challenging.

Examples of partially recrystallized structures visualized by OM, ECC, EBSD and TEM are given in figure 1. By looking at all these partially recrystallized micrographs, a common feature can be noticed namely that recrystallizing boundaries are rough, locally consisting of many protrusions and retrusions with sizes of few to tens micrometres, which reflects that the migration of recrystallizing boundaries is inhomogeneous. Although this feature was reported in the literature even in 1950's (see

figure 1a), not much attention has been paid to these local 'anomalies' until recently. In order to understand the formation of protrusions and retrusions as well as their importance for the boundary migration, quantification methods of individual protrusions/retrusions and correlations between protrusions/retrusions and the neighboring deformation matrix are needed.

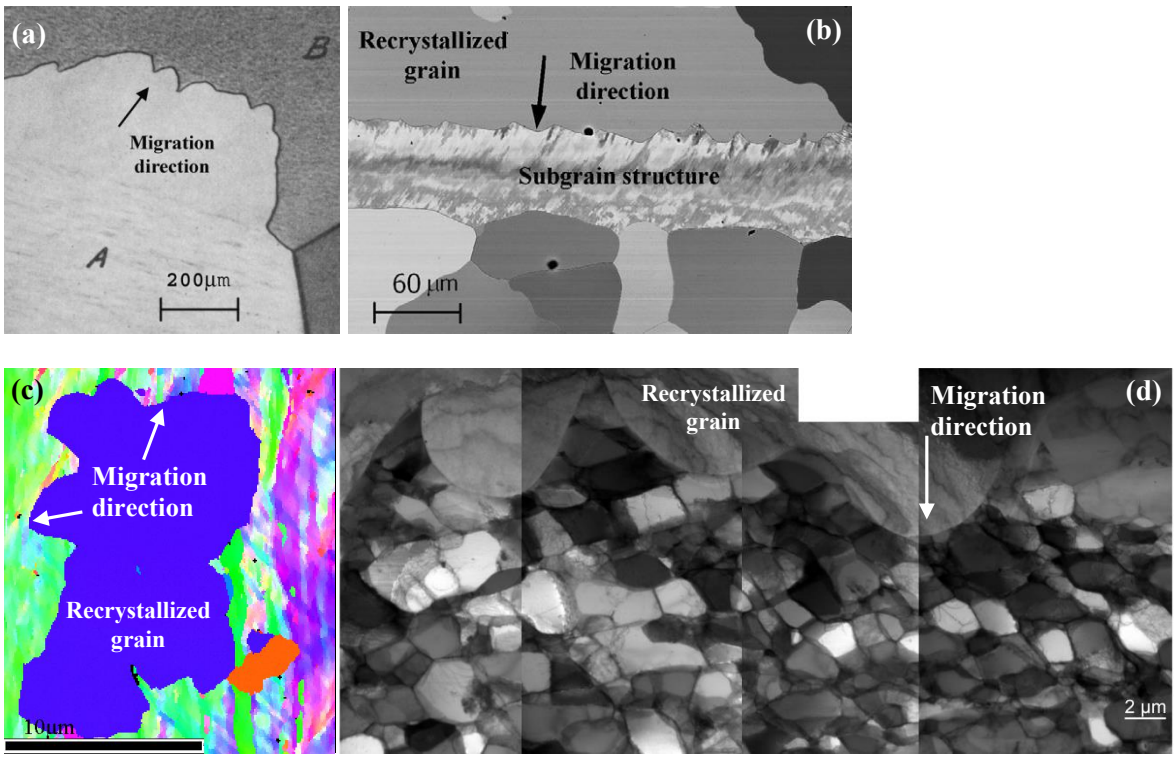

Figure 1. Examples showing rough recrystallizing boundaries in different partially recrystallized materials using different characterizing techniques: (a) optical micrograph showing strain induced boundary migration in high purity aluminium (Reproduced with permission from [13], Copyright 1950, AIP Publishing LLC.), (b) ECC image showing a grain boundary with protrusions migrating into a recovered region during recrystallization of high purity tantalum (body-centered cubic) (Reprinted from [20] with permission from Elsevier), (c) EBSP map of partially recrystallized microstructure of 96% cold rolled pure (99.996%) nickel [21], (d) TEM image showing in detail the rough features on a recrystallizing boundary in a partially recrystallized pure aluminium sample.

2.1. Quantification of protrusions/retrusions

To describe quantitatively protrusions/retrusions, Martorano et al. [22] used a sinusoidal function to simulate a variation in driving force and consequently boundary shape in a numerical analysis of growth during recrystallization. Considering the experimental fact that most protrusions/retrusions do not have a perfect sinusoidal shape, Zhang et al. developed another method, using polynomial equations to fit the shape of protrusions/retrusions, to obtain a more precise quantification of the individual protrusions/retrusions [12, 21]. The method is illustrated in figure 2. Individual protrusions/retrusions are first selected manually from the 2D experimental images, and then the boundary segments are fitted using a 3rd or 4th order polynomial equation. The radius of the curvature of the boundary can then be calculated by:

$$r = (1+\dot{y}^2)^{3/2}/\ddot{y}, \quad (2)$$

where $\dot{y}$ and $\ddot{y}$ represent the first and second derivatives of the selected polynomial equation, respectively. The curvature-based driving force for each protrusion/retrusion is then calculated using equation (3) [1]:

$$F_\sigma = 2\sigma/r, \tag{3}$$

where σ is the grain boundary energy and r is the radius of the curvature of the boundary.

This method can be used to quantify the protrusions/retrusions on recrystallizing boundaries observed with all the characterization techniques mentioned above and as shown in figure 1. Among these micrographs, ECC images are generally the most appropriate ones, considering their high spatial resolution, short acquisition time and easy sample preparation. Only when really small protrusions/retrusions have to be characterized, TEM is needed. In term of automatic grain boundary detection for quantification, however, EBSD maps are obviously the best choice because of the additional orientation information, which helps separating recrystallized grains from the matrix.

As the curvature varies along a protrusion/retrusion on the recrystallization boundaries, the maximum curvature-based driving force, $F_{\sigma,max}$, at the position where the radius of the curvature is minimum is suggested to be used to quantify each protrusion/retrusion [12]. By measuring all the protrusions and retrusions on a boundary, the distribution of $F_{\sigma,max}$ can be obtained. An example of such a distribution is shown in figure 3b, where $F_{\sigma,max}$ values are calculated for all protrusions and retrusions on the boundary in figure 3a. Large spreads of the distribution of $F_{\sigma,max}$ are seen for both protrusions and retrusions, implying large curvature differences between individual protrusions/retrusions. The tail in the distribution for retrusions is much longer than that for protrusions, revealing that retrusions on this boundary are much sharper than protrusions. This type of distribution can be used directly to compare characteristics of different boundaries in the same or different materials, and thereby provide a basis for understanding the correlation of boundary structures and local deformed microstructure in front of the moving boundary, as will be discussed in the next section 2.2.

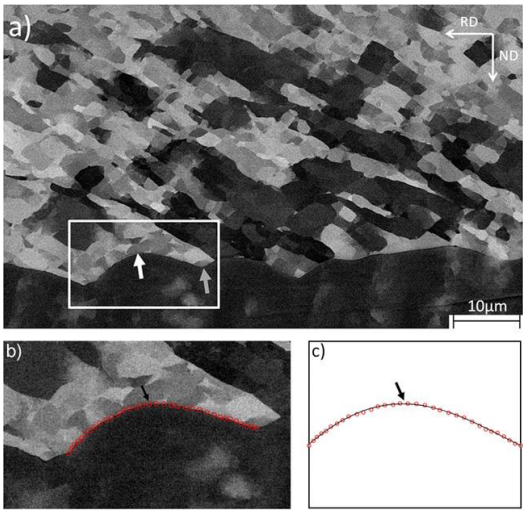

Figure 2. Illustration of the procedure for quantification of protrusions/retrusions. (a) ECC image showing a partially recrystallized microstructure of 50% cold-rolled aluminium annealed at 250 °C for 10 minutes. A white and a grey arrow are used to mark a protrusion and a retrusion, respectively. (b) Enlarged image of the microstructure within the white rectangle in (a), with the boundary segments traced by red circles. (c) The fitting result, as shown by the thick black line. Black arrows in (b) and (c) are used to mark the place where the boundary curvature is minimum and thus the dragging force is maximum. [12]

A drawback of this method is that it is a time consuming process to obtain the distributions of $F_{\sigma,max}$, even for one boundary, as the boundary is determined manually. Recently, Sun et al. have developed a fully automatic method, where a parameter called area integral invariant is used to quantify protrusions/retrusions on a boundary and thereby to quantify the boundary roughness. A detailed description of this method can be found in this proceeding [23].

2.2. Correlation to the deformed microstructure

To correlate the local protrusions/retrusions to the local deformed microstructure in front of the boundary, quantitative crystallographic information over a large area are required. For this purpose,

EBSD generally is the best choice. But to optimize the data collection process, EBSD can be used together with ECC: ECC for quick, high-resolution characterization of protrusions/retrusions and EBSD for characterization of deformation microstructures on a coarser scale.

A simple calculation has been made to correlate the average maximum curvature dragging/driving forces from protrusions/retrusions (i.e. $<F_{\sigma,max}>$ for protrusions/retrusions) with the average stored energies in the deformed microstructure in front of the boundaries [21]. The stored energy is estimated based on EBSD maps. In that work, $<F_{\sigma,max}>$ for protrusions was calculated based on sinusoidal equations. A more precise calculation of $<F_{\sigma,max}>$ for both protrusions and retrusions using the method described in equations (2) and (3) has been conducted in the present work, and the correlation is shown in figure 4. For protrusions, an overall trend can be seen: higher average stored energy leads to higher $<F_{\sigma,max}>$, although with a large scatter. For retrusions, the magnitude of $<F_{\sigma,max}>$ is much larger (note the scale difference in figure 4a and 4b), and the spread is larger.

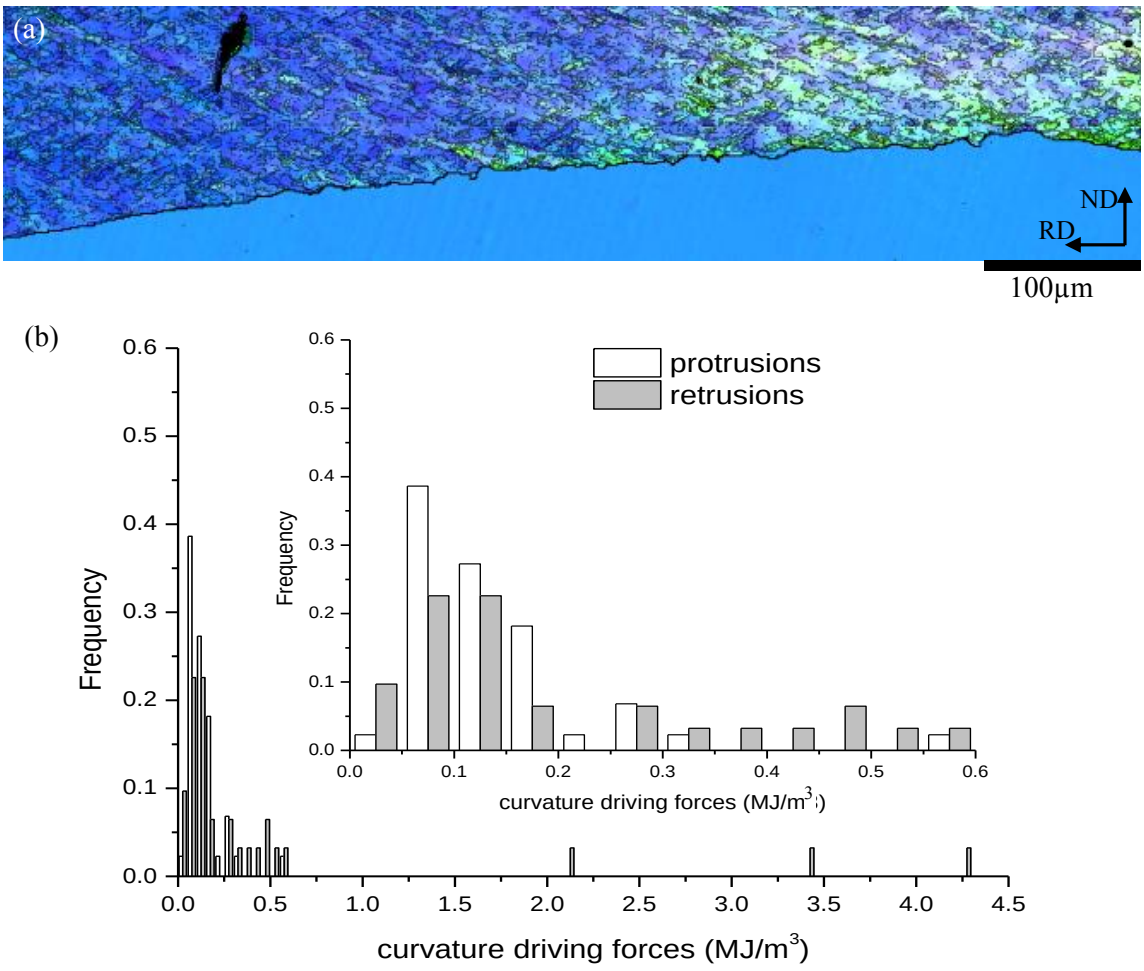

Figure 3. (a) EBSD map showing a long rough recrystallization boundary in 50% cold-rolled aluminium annealed at 250 °C for 10 minutes. (b) Distribution of $F_{\sigma,max}$ for both protrusions and retrusions along the boundary in (a). Insert in (b) showing the details of the distribution in the range of 0-0.6 MJ/m^3.

It has to be noted that the curvature of a protrusion provides a dragging force for the boundary migration. The size of protrusions can therefore not be so large, as the curvature dragging force cannot exceed the local driving force from the stored energy in the deformed matrix, i.e. the protrusion size is limited by the magnitude of the local stored energy. On the other hand, the curvature of a retrusion

provides an extra driving force for the boundary migration to be added to that of the stored energy in the deformed matrix. The retrusion size is therefore not limited by the stored energy. However, why the retrusions on some boundaries can become so large is not trivial to understand, considering the fact that the curvatures of retrusions can provide much larger driving forces than the stored energy in the deformed matrix, and that neighboring stagnated segments of the boundary may be pulled forward. Simple energy balances as that suggested for the protrusions may therefore not be valid.

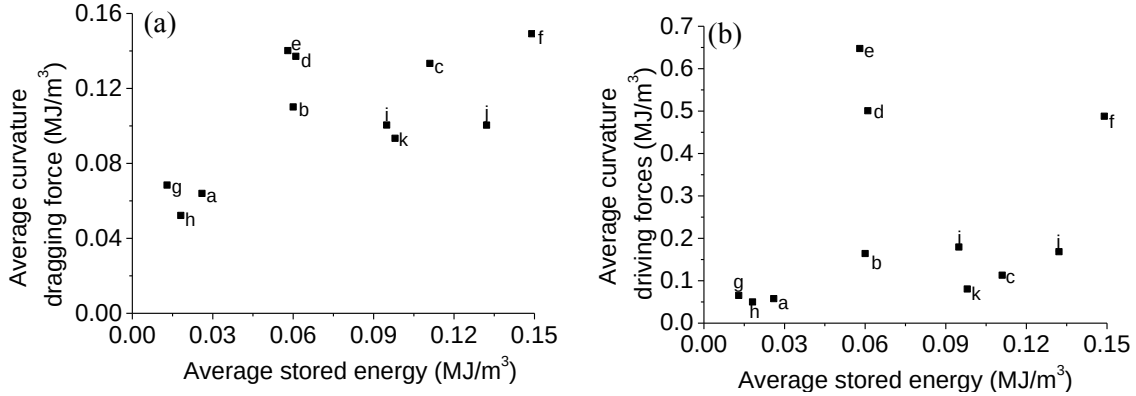

Figure 4. Average curvature dragging (a) and driving (b) forces as a function of the average stored energy in the deformed matrix for 11 different recrystallizing boundaries (marked with letters a-k) in partially recrystallized 50% cold-rolled aluminium annealed at 250 °C for 10 minutes.

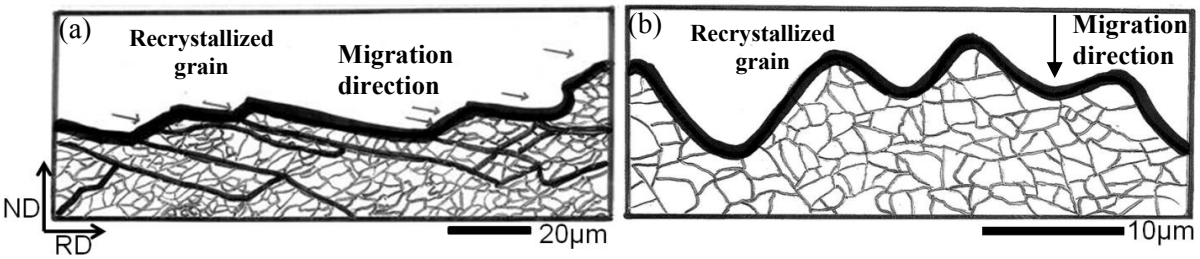

Figure 5. Sketches of protrusions and retrusions on recrystallization boundaries in 4N pure Al (cr 50% and annealed at 250 °C for 10 minutes). (a) Sketch based on ECC image showing saw-tooth shaped protrusion. The fat lines in the deformation microstructure represent extended dislocation boundaries across which a significant contrast variation is observed. The arrows indicate the expected direction of boundary migration. (b) Sketch based on a TEM image showing rounded protrusions. [24]

Several reasons may explain the large scatter in figure 4. (i) Both the sizes of protrusions/retrusions and the local stored energy vary from place to place, even along the same boundary. (ii) The deformed microstructures are typically heterogeneous, depending strongly on the grain orientations. Therefore, even for two deformed grains with similar stored energy, the deformed microstructures may be completely different, and hence the resulting protrusions/retrusions may be of different types. For example, round and saw-tooth types of protrusions have been observed along different recrystallizing boundaries in partially recrystallized pure aluminium depending on the local microstructure in front of the recrystallizing grains (see figure 5). (iii) The protrusions/retrusions and stored energies are characterized based on 2D images. (iv) According to equation (1), variations in boundary mobility may also be a reason. Lower mobilities for some segments may lead to large retrusions. (v) As the analysis in figure 4 is based on statistical characterizations, the real deformation microstructures that result in the observed protrusions/retrusions have at least partly been consumed. The stored energy calculated in figure 4 is therefore not the actual driving force that led to the formation of protrusions/retrusions.

To clarify these possibilities, future work may include: correlating each individual protrusions/retrusions with *local* stored energy in the deformed microstructure to clarify point (i) above; morphological analysis of the recrystallizing boundaries and the deformed microstructures to investigate possible correlations and thus clarify point (ii); the unknown variations in the third dimension have to be investigated by 3D (x, y, z) characterizations (point (iii) above); points (iv) and (v) can be analyzed by dynamic studies.

3. 3D (x, y, z) static characterizations

3D (x, y, z) characterization techniques can generally be divided into two groups: destructive ways using serial sectioning, and non-destructive ways using e.g. high energy X-rays. The destructive ones leading to static characterization are discussed in this section, while non-destructive ones will be discussed in section 5 in connection with dynamic 3D studies, because the non-destructive techniques offer this possibility.

Characterizations of 3D volumes using destructive serial sectioning are normally achieved by repeating two processes: sectioning and microstructural characterization. For the microstructural characterization, microscopy, e.g. OM, ECC and EBSD can be used (e.g. [25, 26]). Earlier, OM was the main characterization tool, but nowadays EBSD is more and more used. The sectioning process can be conducted using focused ion beam (FIB) inside an SEM (e.g. [27]) or using electro- (e.g. [28]), chemical polishing (e.g. [29]) or laser ablation (e.g. [30]). One of the advantages with FIB and laser ablation is a relatively high resolution (down to a few nanometres at the best) for each milling layer, thanks to the high precision of the beam. With commercial software the whole characterization process can be automated, which reduces significantly the amount of work for later alignment between layers. The advantage with manual mechanical, electro- or chemical polishing is that there is no limit in the size of the characterization area at each layer. The minimum sectioning thickness is, however, much coarser than with FIB and laser. Even with the most advanced automatic characterization system, such as Robo-Met. 3D [31], the best resolution can only be 200 nm, while with a human-based polishing process 2 μm at the best is more realistic.

Among all the 3D studies published, deformation microstructures are more often characterized than recrystallization (e.g. [32, 33]), and few papers relevant for local grain boundary migration are published. One example is given in the following.

3.1. 3D characterization of recrystallization boundary, using FIB

To visualize the 3D shape of a recrystallizing boundary, a 3D microstructure containing a recrystallizing boundary separating a recrystallized grain and deformed matrix has been characterized using FIB as a serial sectioning milling tool and EBSD for microstructural mapping. In total, 40 layers with 0.5 μm resolution along all three directions have been obtained (see figure 6a) [34]. The characterized volume has a size of 50 × 60 × 20 μm^3. The 3D morphology of the recrystallizing boundary can be easily revealed because of the difference in orientations across the boundary. The 3D rendering of the recrystallizing boundary in figure 6b shows clearly the heterogeneity of protrusions/retrusions in different sample directions. This data showed that in at least this sample the 3D protrusions/retrusions are not isolated peaks but elongated ridges along TD. This result indicates that an estimation of protrusion/retrusion sizes and curvatures based on 2D microstructural investigations in the RD-ND section for cold rolled samples may not deviate too much from the true 3D results (at least for the present example).

By having the fine spatial resolution, the deformed microstructures can also be reconstructed in 3D, and the 3D influence of deformation microstructure on the formation of protrusions/retrusions can be examined. The 3D result clearly reveals that the dislocation boundaries are aligned almost parallel to the TD direction (see figure 7), which indicates that the actual 3D bands in the deformed microstructure can be reasonably represented by 2D bands seen on the RD-ND section. The protrusions/retrusions appear to be flatter in the RD-TD plane compared to the RD-ND plane, which supports the suggestion that the extended banded deformation structure along TD affects the evolution of protrusions/retrusions.

With this data set, the characteristics of the recrystallization boundary can be obtained. Misorientation analysis shows no systematic difference between the boundary segments of the protrusions and retrusions. The boundary plane normal of the recrystallizing boundary can also be obtained. Detailed correlation of the boundary plane normal with the local deformed microstructure can therefore also be made. One drawback of this result is the volume characterized is relatively small and thus not good for statistical analysis as that conducted based on the 2D images. Furthermore, the destructive sectioning does not allow following the boundary migration dynamically.

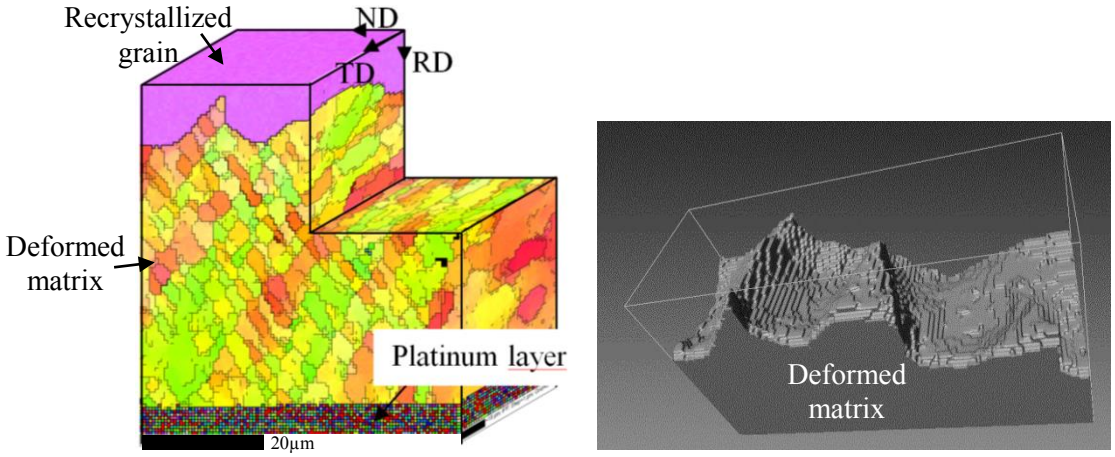

Figure 6. Example showing the 3D characterization using FIB as milling tool inside a SEM. (a) 3D volume showing the reconstructed microstructure around a recrystallization boundary in partially recrystallized pure aluminium (cr 50% and annealed at 250 °C for 10 minutes). (b) Top view of the recrystallizing boundary surface, the volume visualized as a solid is the deformed matrix. The bottom random colored layers in (a) are caused by platinum deposition. [34]

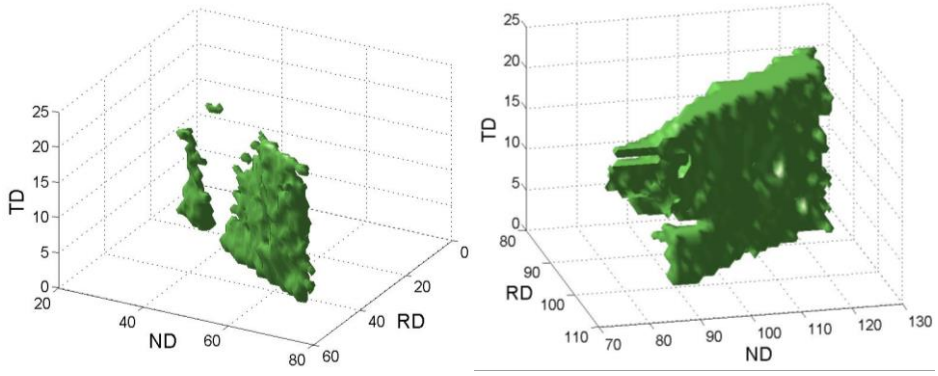

Figure 7. Examples showing two 3D alignment of bands of dislocation boundaries subtracted from the deformed matrix in figure 6a, where 2° is used to detect dislocation boundaries. [34]

4. In-situ/ex-situ 2D (*x*, *y*, *t*) characterizations

Dynamic studies following in situ or ex situ the boundary migration process are crucial for understanding the migration mechanisms. The direct observations from such studies can avoid the so-called 'destroy-evidence' problem [35], and thus be used to test mechanisms or theories as those obtained based on the 2D post-mortem analysis e.g. those given in section 2. Moreover, in-situ/ex-situ studies can provide new possibilities for quantification of *local* microstructural changes during recrystallization, e.g. *local* boundary migration rate, local stored energies for the migration, *local* boundary misorienations, and recovery in the deformation matrix.

To perform in-situ/ex-situ characterization, all 2D characterization techniques can be used. TEM and high voltage TEM were used intensively in the 1970-80's (e.g. [36, 37]). Because only relatively small areas can be observed using TEM, most of these investigations are focusing on the early stages of nucleation. As only thin foils can be probed by TEM, the investigations may be affected by the two free surfaces and the wedge shape of the thin sample area. The phenomena observed may therefore not represent the true bulk behavior.

Since EBSD became a common characterization technique, more and more in-situ/ex-situ recrystallization studies are conducted with EBSD instead of TEM. Although the spatial resolution does not compare with that of TEM, there are several advantages in using EBSD for in-situ/ex-situ studies. Besides those mentioned in section 2, a large characterization area, only one free surface, easy sample handling, and resistance to sample buckling are additional advantages with EBSD compared to TEM for in-situ studies. As the sample preparation for ECC characterization is the same as for EBSD, ECC has also been used for in-situ/ex-situ studies, though less frequently than EBSD because it does not provide enough crystallographic information. The time resolution for in-situ/ex-situ ECC characterizations can be much higher than that for EBSD. It may therefore be beneficial to combine EBSD with ECC for in-situ/ex-situ studies: using the EBSD mapping with a sufficient angular resolution for calculation of boundary misorientations and local stored energies, while using ECC images to have both a higher spatial resolution and a faster data acquisition of the microstructural evolution.

One of the difficulties to combine EBSD mapping with ECC imaging is the drift problem, which typically results in non-linear spatial distortion in the EBSD maps [38]. Due to the distortion, features in the EBSD maps may not directly be registered with those in the ECC images. To solve this problem, a correction method, thin plate spline, has been developed to correct the spatial distortion in the EBSD maps [38]. After correction, EBSD maps can easily be fused with ECC images for quantitative analysis.

In recent years, both EBSD and ECC have been used to follow recrystallization process in situ/ex situ (e.g. [40-43]). Many of those studies are, however, of demonstration types focusing on methodology and qualitative description of recrystallization process but not so much on quantification. Even in the latter case, most of the works are still based on the average properties of the whole samples or over the whole characterization areas [41, 42, 44]. A few examples, in which quantitative analyses of boundary migration have been conducted on the local scale, are summarized in the following.

4.1. Ex-situ ECC studies of boundary migration

The migration of a recrystallizing boundary in partially recrystallized high purity aluminium has been followed using the ECC technique, with the aim of quantifying local protrusions/retrusions and understanding their effects on boundary migration [12]. The boundary migration process can be seen in figure 8, where numbers are used to identify protrusions and retrusions. The results reveal that the migration of recrystallization boundaries is quite inhomogeneous and differs from place to place: some boundary segments move faster while others move slower. Also some segments migrate in a stop-go type of fashion, while others migrate during all annealing steps (see figure 8d).

Detailed quantification of protrusion and retrusion sizes using the methods described in section 2.1 has shown that during the whole investigated migration period, the values of $F_{\sigma,max}$ for protrusions are mainly in the range of -0.05~-0.2 MJ/m^3, whereas for retrusions $F_{\sigma,max}$ can be much higher, with most of them in the range of 0.2~1.0 MJ/m^3. This suggests that during the migration process the magnitude of both the dragging and driving forces from the evolving protrusions and retrusions, respectively, can be of comparable magnitude to that from the energy stored in the deformed matrix. Equation (1) is therefore suggested to be modified as:

$$v = M \cdot (F_S + F_\sigma), \tag{4}$$

where F_S and F_σ are the driving force contributions from the stored energy of the deformed structure and boundary curvature, respectively. The ex-situ results have also confirmed that during boundary

migration the protrusions are relatively small, and the protrusions can become stationary at some stage (e.g. protrusion no. 1 in figure 8) once the dragging force from protrusions, F_σ, counterbalanced the driving force from the stored energy, F_S according to equation (4). These observations have further shown the importance of F_σ for understanding local boundary migration.

It is however rather difficult to understand the local migration behavior of retrusions based on equation (4), as both driving forces from stored energy and from boundary curvature of retrusions have positive signs, and the sum of both is much higher than the driving force for the migration of protrusions. It is clear that if the local driving force in front of a retrusion is low, the retrusion may not move forward and thus develop to become very large [45, 46]. This is however not the situation here. For example, it is found that during the whole annealing process followed here, segments at the tip of retrusion no. 2 only migrate when $F_{\sigma,max}$ is higher than 0.55~0.60 MJ/m^3 [12]. It is possible that the mobility for segments at retrusion no. 2 is smaller than their neighboring, as the contrast of the deformed cells in front of these segments (as marked by the ellipse in figure 8a) is different from their neighboring. But how different the mobility can be, and how the mobility differences can lead to stagnation of the boundary segments cannot be investigated by this experiment, as quantification of boundary characteristics and stored energy in the deformed matrix cannot be obtained based on ECC images.

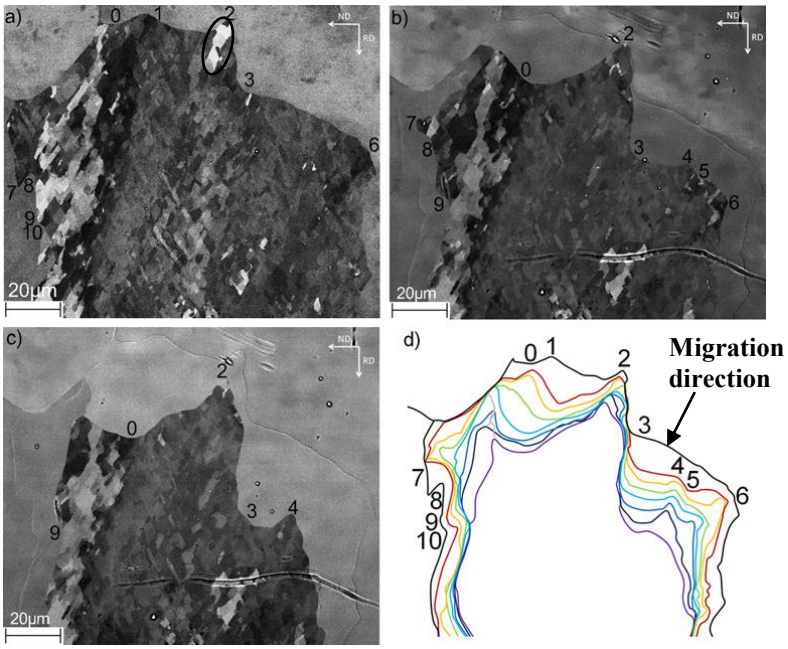

Figure 8. ECC images showing the microstructural evolution of 50% cold rolled aluminium during annealing at 250 °C for: (a) 10 minutes; (b) 10+3x15 minutes; (c) 10+6x15 minutes. (d) Locations of the recrystallization boundary during the entire annealing sequence. Specific protrusions and retrusions are identified using numbers. The ellipse in (a) marks deformation cells with a different contrast from their neighbors. [12]

4.2. Combining EBSD and in-situ ECC to follow boundary migration

Ex-situ EBSD studies have been carried out to follow the growth of individual grains during recrystallization in heavily cold rolled nickel [47]. The local microstructures that were consumed during annealing were extracted and detailed misorientation analyses of moving boundaries and non-moving boundaries were carried out. The results have, however, shown that even neighboring boundary segments, with very similar misorientations to the neighboring deformed microstructure and with similar driving force (F) from the deformed matrix, can behave quite differently [47]. The EBSD

mapping step size for this study was coarse (2 μm), and effects of local deformation microstructures on the growth could therefore not be revealed.

Very recently, new experiments have been conducted to follow the local boundary migration: EBSD was used to characterize the starting microstructure and the boundary migration was followed using ECC during in situ annealing inside the SEM [48]. Figure 9a and 9b show a subset of the starting microstructures, while figure 9d shows 7 boundary traces that have been analyzed in detailed. The general boundary migration pattern is similar to that found in the above mentioned ex-situ studies. It is seen, that after the second time step the two ends of the boundary remain fixed, where long, flat boundary segments develop, which do not migrate further during the entire duration of the annealing experiment. In between these fixed points, the migration of the recrystallizing boundary is quite heterogeneous: many small protrusions/retrusions form during the migration, and the migration velocity varies in space and time, with fast migration observed in particular during time interval #2. The misorientation analysis has shown that not much difference is observed between the migrating and non-migrating boundary segments [48].

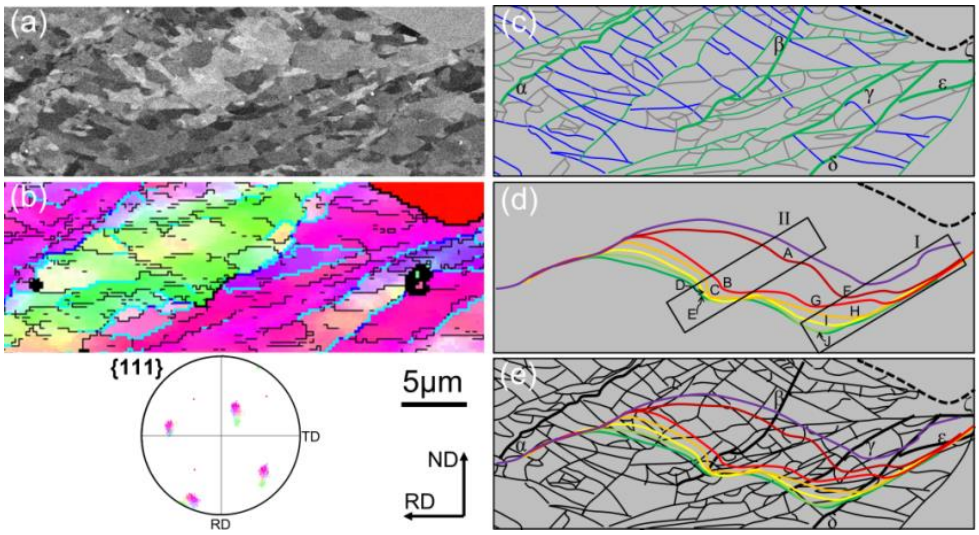

Figure 9. EBSD and ECC techniques used in combination to characterize the microstructure and to follow in situ the boundary migration in partially recrystallized pure aluminium (cr 50% followed by rolling at liquid-nitrogen temperature to a total reduction of 86%) during annealing at 50 °C. (a) ECC image, (b) EBSD map and (c) sketch based on ECC image in (a) showing the microstructure in the area where detailed boundary migration are analyzed. (d) Traces of the positions of the recrystallizing boundary during the first seven 100 s time steps. Box I and II mark local areas where detailed analysis is carried out. Letters A-J are used to identify protrusions. (e) Non-colored image of the deformed microstructure (from c) superimposed with recrystallizing boundary traces shown color. In (c) and (e) boundaries containing segments with misorientation >10° are highlighted by thicker lines and marked by α-ζ in (c). [48]

By correlating the boundary traces with the deformed microstructure (figure 9e), it is evident that the coarsely spaced dislocation boundaries, marked by Greek letters in figure 9c, which have higher misorientations, have dominated the migration process and stimulated the formation of protrusions (see figure 10a). The higher local stored energies induce larger protrusions, and the maximum curvature-based dragging forces from protrusions are typically smaller than the local stored energies, with one exception for protrusion C. It should be noted that only the maximum curvature dragging force is used for the protrusions, while the stored energy is calculated as an average energy density over the small area under each complete protrusion profile. According to equation (4), the protrusions B, C, D should have a reduced migration rate or stop moving at next annealing step, and protrusions A,

F, G can continue migrate during next annealing step. This agrees well with the experimental observations, i.e. the migration is understood qualitatively.

However, quantitative understanding of the migration is more challenging. Even when the local net curvature dragging/driving forces from protrusions/retrusions are included in a detailed quantification of boundary migration, a large scatter between the migration velocity, v and the modified driving force, $F_S + F_\sigma$ is found (see figure 10b), where a significant deviation from a simple straight line relationship as predicted by equation (4) is observed. Several reasons have been suggested to understand this result [48]. Among those, lack of knowledge about the appropriate value of mobility, M, which may be complex and may depend on many parameters, is suggested to be the main factor to be examined in future experiments. Also the fact that individual boundary segments are strongly affected by the motion of neighboring segments has also to be considered. Both advanced modeling and 3D experimental tools are required to clarify these issues.

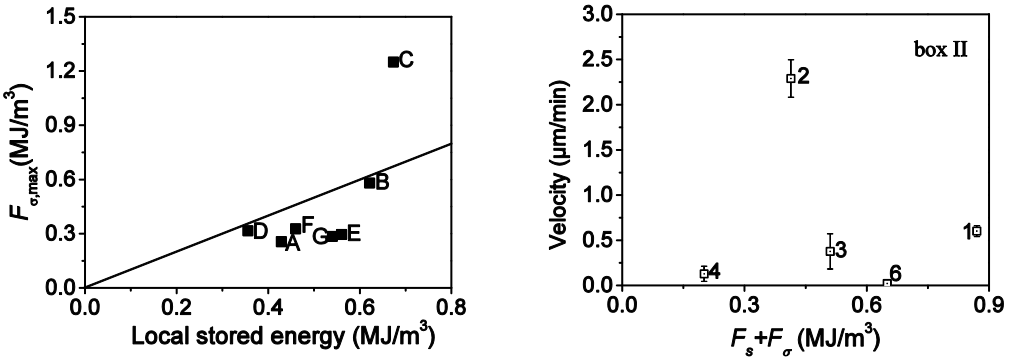

Figure 10. (a) Maximum curvature dragging forces ($F_{\sigma,max}$) from the protrusions A-G (marked in figure 9d) against the local stored energies calculated from the deformed microstructure consumed by the protrusions. (b) Migration velocity of the recrystallizing boundary as a function of total driving force, $F = F_s + F_\sigma$, for boundary segment in box II in figure 9d for each time interval. Numbers show the time intervals. [48]

5. In-situ/ex-situ 3D (x, y, z, t) characterizations

In the last 15-20 years, two major groups of non-destructive 3D characterization techniques have been developed and used for recrystallization studies, namely 3DXRD techniques (e.g. [49, 50]) and differential aperture X-ray microscopy techniques (also called 3D X-ray crystal microscopy (3DXRM)) (e.g. [51]). With these techniques, the boundary migration can be traced in situ/ex situ in 3D, so that full boundary information described by 5 parameters (3 for misorientation and 2 for boundary plane normal) can be obtained, and the influence of 3D deformed microstructure on boundary migration can be directly visualized.

The 3DXRD techniques utilize typically monochromatic, high energy, high brilliance, and hard synchrotron X-rays at large third generation synchrotron facilities. For reconstruction of the 3D volume, 'tomographic' reconstruction algorithms are used for analysis of the diffraction data recorded using detectors at different distances to the sample. Several operation modes can be chosen to optimize spatial, angular or time resolution in a 3DXRD experiment. Typically, due to limitation of the detector resolution to ~1 μm, the spatial resolution can be fine-tuned in the range of ~1-5 μm depending on the experimental requirements. Time resolution of a few minutes to a few hours allows in-situ or interrupted in-situ studies. Angular resolution is ~0.1°. However, the 3DXRD techniques are currently still not capable of resolving deformed microstructure, especially for deformation >20% [10, 49, 50].

Very recently, based on the 3DXRD techniques, a new concept ─ dark-field X-ray microscopy (DFXRM) ─ has been developed and implemented [52]. This technique utilizes an objective (typically consisting of many compound refractive lenses (CRLs)) to magnify a diffracted beam by a factor of typically 10-20. With this technique, 3D maps of orientations within both individual deformed and recrystallized grains with a spatial resolution of ~300 nm have been achieved [52].

The 3DXRM techniques utilize a focused, polychromatic synchrotron X-rays with energy of 5-30 keV [51, 53]. A Pt wire is used as a differential aperture to differentiate diffraction signal from different sample depth along the beam, and crystallographic information is resolved by indexing the Laue diffraction patterns at each depth [51]. Practically, due to limitations from the imperfection of the focusing mirror, the spatial resolution is ~500 nm. As the 3D mapping is in a scanning mode, the time resolution of this technique is normally poor. Nowadays, to map a reasonable volume can take up to 2-3 days. Therefore only interrupted in-situ or ex-situ studies are possible. The angular resolution is ~0.01°. Using these techniques, 3D deformed microstructures in deformed samples (<50% deformation) have been resolved with submicrometre resolution [54].

Both groups of techniques have been used for studies of local boundary migration. The achievements in understanding of recrystallization boundary migration as well as future potentials are summarized in the following.

5.1. Watching growth of individual grains into a lightly deformed single crystal

With 3DXRD techniques, the first state-of-the-art experiment to follow the growth of a recrystallized grain into a lightly deformed Al1050 single crystal during in situ annealing was reported in 2004 [11]. Rough boundaries and very heterogeneous migration patterns of individual boundary segments were observed in 3D, through the whole growth period. For example, the formation and evolution of protrusions/retrusions on the growing boundary and stop-go type of motion were for the first time demonstrated in that experiment to be a bulk behavior and not artifacts from 2D observations. The spatial resolution of this 3D experiment was about 5 µm along the *x*, *z* direction and 20 µm along the *y* direction (beam direction). [11]

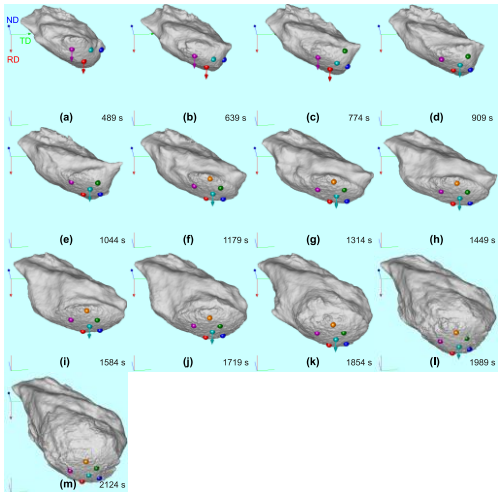

Figure 11. Snapshots of a grain at different times during its growth through the deformed matrix of a near cube oriented single Al crystal. Protrusions/retrusions are seen on many boundary segments and the dots and arrows show the formation and migration of a coarse scale facet. The dimension is given by the tripod, with arms 42 µm long. (a)-(e) are annealed at 290 °C, while (f)-(m) are annealed at 300 °C. [55]

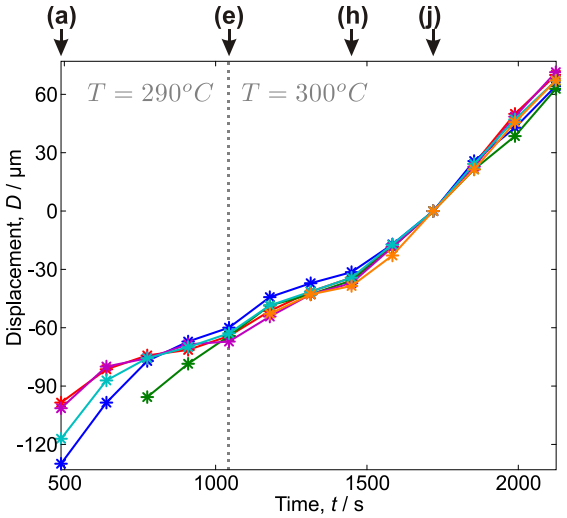

Figure 12. Displacement-time curves obtained from the 3D reconstructions along the set of parallel lines indicated in figure 11. The displacements of local grain boundary segments are characterized by the distances of the successive intersection points along the parallel lines to their reference positions (which are the positions of the intersection points at 1719 s). [55]

To overcome this limited spatial resolution, the topo-tomography technique, which is a kind of 3DXRD, has recently been used to follow the growth of a recrystallized grain in a deformed single crystal of near cube orientation [55]. Figure 11 shows the grain after different annealing times [55]. As this technique gives a better spatial resolution of 1.4 µm along all directions, details of the local

protrusions/retrusions and facets on the boundary are clearly visualized, and quantifications of boundary morphology are possible. For example, the evolution of the facet, marked by color dots in figure 11, has been analyzed (see figure 12). It is seen that the facet develops only after a certain annealing time and afterwards grows as a unity. An interesting observation is that the facet is not parallel to any of the crystallographic {111} or {100} planes, but parallel to the macro sample RD direction. To understand how this larger than 100μm-size facet develops and why it grows preferentially along RD require detailed characterization of the deformed microstructure, which is still not possible with this technique.

5.2. Ex-situ studies of boundary migration with 3DXRM.

As the 3DXRM techniques enable resolving deformed microstructures at the submicrometre scale, the 3D microstructure shown in figure 6 can be obtained non-destructively, and the migration of a 3D boundary and its correlation to the 3D deformed microstructure can also be obtained. The authors have recently conducted successfully such type of experiments. Both the deformed microstructure and recrystallized grains separated by a recrystallizing boundary have been indexed in 3D with a spatial resolution of 1μm along all directions, and the migration of the boundary has been followed by ex situ annealing. With this 4D data set, the larger goal of studying effects of both the misorientations (angle/axis pair) and the boundary plane normals for the 3D boundary can be achieved. Also possible effects of the 3D deformed microstructure on the migration can be examined. The data processing is in progress.

5.3. Recrystallization boundaries studied by DFXRM

With the ability to resolve both deformed microstructure and recrystallized grains, the DFXRM technique is also a powerful tool for 4D recrystallization studies. Very recently a layer (200 nm thick) of a recrystallized grain in a partially recrystallized Al1050 sample has been characterized using this technique [56]. The diffraction signal from the investigated recrystallized grain is magnified 18 times using Be CRLs as objective lens. The spatial resolution, which is limited by the optical performance of the lens, is ~200 nm. The ultra-high angular resolution of ~0.005° allows detailed characterization of e.g. very low angle boundaries. The full 3D shape of the grain can be reconstructed layer by layer using this technique, and the growth of the grain can be followed by repeating the 3D reconstruction after different annealing times. As the technique can also resolve the deformed microstructure with high spatial resolution, the effects of the deformed microstructure on the growth can in theory be investigated [56].

6. Conclusions and outlook

6.1. Evaluation of the characterization techniques

The present paper has demonstrated essential potentials of advanced characterization techniques for understanding the recrystallization boundary migration process. All the 2D characterization techniques mentioned in the paper have become standard tools in most research laboratories. Combined with the fact that it is relatively easy to learn to operate these techniques, they therefore are important ‘work horses’ for studies of boundary migration during recrystallization. The drawback with 2D characterization is it only reveals a 2D section of the whole bulk sample. Although statistical quantification of average parameters can be obtained using stereological methods, local parameters for individual grains or boundaries are always suffering from uncertainties in the third dimension. Similarly, kinetic information can be obtained by analyzing statistical results from a series of samples with e.g. different recrystallization fractions. But these analyses are post-mortem, and sometimes suffer from the so-called ‘destroy-evidence’ problems.

Destructive 3D (x, y, z) characterization techniques have had a renaissance and have become more frequently used for materials science research in recent years. In many scientific studies, the need for 3D (x, y, z) techniques has been demonstrated, to obtain a complete picture of the microstructure, and to remove the bias, uncertainties, and sometimes misinterpretations from 2D characterizations. In

some cases 3D data sets provide completely new findings. The efforts that are needed to collect 3D data sets are however large compared to those for a 2D data set. First the access to equipment that enables 3D characterizations is still relatively limited. Furthermore significant experience is required to obtain good 3D data sets. Also the data acquisition time is long. To have a reasonable volume characterized using FIB milling may take days or weeks, while with manual milling it may take weeks to months. Finally, the destructive methods inherently do not allow any dynamic studies. Data post processing of 3D data sets (e.g. data alignment and segmentation) and visualization are still typically challenging due to the large data set and lack of suitable software. Currently, several open source software, e.g. Image J [57], Dream3D [58] and MTEX [59], have been developed for handling 3D data sets, which may ease the situation, but more functionalities have to be developed.

Compared to the 3D (x, y, z) characterizations, the efforts required for conducting good in-situ/ex-situ 2D (x, y, t) studies are less, especially for ex-situ studies, for which no heating device inside e.g. the SEM is required. With in-situ/ex-situ studies, so-called 'destroy-evidence' problems are solved. Similar to the 3D (x, y, z) characterizations, there is, however, still a lack of in-house or commercial software that allow quantifications of local microstructural changes. Additionally, this type of studies always suffers from surface problems [60], which in some cases may be critical for interpreting the results.

The synchrotron 3D techniques are no doubt the most powerful tools for recrystallization studies. They provide unique possibilities for non-destructive in-situ 3D studies, from which the microstructural evolution can be revealed in full 4D. The drawback of these techniques is related to the very limited access to synchrotron facilities. In order to get beam time, a high scientific level proposal and cutting edge type of experiments are typically required. Even if beamtime is allocated (typically maximum a week), the success rate of synchrotron experiments may be low, due to complex instrumentation, and other unexpected problems. Therefore very careful preparation of the experiment is highly recommended, which typically can take half a year or more. Another major drawback of synchrotron experiments is that the limited beamtime does generally not allow for series of experiments and thus not for very systematic studies of effects of metallurgical parameters on, e.g. boundary migration.

Currently, the spatial resolutions of the non-destructive 3D synchrotron techniques are all lower than those of the 2D electron microscopy techniques. For the 3DXRM techniques, the spatial resolution is limited by the focusing mirror, i.e. by the perfection of the mirror. Nowadays, the best ultra-precise K-B mirror fabricated by JTEC Corporation (a spin-off company from Osaka University) can focus hard X-rays at the sub-100 nm level [61]. With this type of mirror installed in the near future, the 3DXRM techniques will allow research of boundary migration at the nanometre scale. Similarly, with better objective lenses fabricated in the future, a spatial resolution of 10-30 nm can in theory be achieved with the new 3DXRD technique, DFXRM. These further advancements of synchrotron techniques will in the future allow recrystallization studies for highly strained nanostructured materials.

6.2. Recrystallization boundary migration

The present paper has demonstrated that local boundary migration is a complex process. It is evident that the local variations within the deformation microstructures are very important for boundary migration during recrystallization. A better understanding of mobilities for a recrystallizing boundary is essential but poorly understood. It remains as open question if one can really operate with simple mobilities in the investigations of local boundary migration during recrystallization. More work has to be done to solve the problems we are facing and to advance the understanding of local boundary migration. Suggestions include:

- More 2D (x, y) and 3D (x, y, z) experimental characterizations of recrystallization boundaries and the local deformation microstructures in front have to be conducted, in order to correlate the local microstructural parameters, e.g. misorientation angles and spacings of the dislocation boundaries, with the local protrusions/retrusions along the boundaries. In this respect,

deformed grains oriented differently, different deformation strains, different annealing temperatures and different materials have to be included.

- More in-situ/ex-situ 2D (x, y, t) and 3D (x, y, z, t) experiments have to be conducted. From such experiments one could try to appropriately quantify boundary mobilities using local boundary migration velocities and local stored energy.
- Computer modelling should be included in the interpretations of experimental results and in defining the most critical experiments to be done. For example using phase-filed modelling to investigate the effects of local microstructural parameters in idealized deformed structures on the boundary migration [45, 46]. Currently, molecular dynamics has been used to determine boundary mobilities (e.g. [62, 63]). Direct comparison between experimental and simulation results will be of importance.
- Currently, the effects of residual stresses in the deformed microstructures are to the authors' knowledge not considered in recrystallization studies. Whether the formation of protrusions/retrusions at different length scales are affected by residual stresses has to be quantified. Here one may choose to focus first on materials with graded structures, in which the residual stresses may be pronounced.

Acknowledgements
The authors gratefully acknowledge the support from the Danish National Research Foundation (Grant No DNRF86-5) and the National Natural Science Foundation of China (Grant No. 51261130091) to the Danish-Chinese Center for Nanometals, within which this work has been performed.

References

[1] Haessner F 1978 *Recrystallization of metallic materials.* (Stuttgart: Dr. Riederer Verlag GmbH.)
[2] Gottstein G and Shvindlerman L S 2010 *Grain boundary migration in metals: Thermodynamics, Kinetics, Applications*, (London: CRC Press Taylor & Francis Group)
[3] Vandermeer R A, Juul Jensen D and Woldt E 1997 *Metall. Mater. Trans.* **28A** 749-54
[4] Cahn J W and Hagel W C 1963 *Acta Metal.* **11** 561
[5] Juul Jensen D 1992 *Scripta Mater*. **27** 533
[6] Lu Y, Molodov D A and Gottstein G 2011 *Acta Mater.* **59** 3229-43
[7] Hansen N and Juul Jensen D 2011 *Mater. Sci. Techno.* **27** 1229-40
[8] Huang X and Winther G 2007 *Phil. Mag*. **87** 5189-214
[9] Schwartz A J, Kumar M, Adams B L and Field D P 2009 *Electron Backscatter Diffraction in Materials Science*, (New York: Springer)
[10] Poulsen H F 2004 *Three-Dimensional X-Ray Diffraction Microscopy, Mapping polycrystals and their dynamics* (Berlin: Springer)
[11] Schmidt S, Nielsen S F, Gundlach C, Margulies L, Huang X and Juul Jensen D 2004 *Science* **305** 229-32
[12] Zhang Y B, Godfrey A and Juul Jensen D 2011 *Scripta Mater.* **64** 331-4
[13] Beck P A, Sperry P R and Hu H 1950 *J. Appl. Phys.* **21** 420-5 doi: 10.1063/1.1699676
[14] Joy D C, Newbury D E and Davidson D L 1982 *J. Appl. Phys.* **53** 81-122
[15] Humphreys F J 2001 *J. Mater. Sci.* **36** 3833-54
[16] Barnett M 2013 *Recrystallization and grain growth V* (Switzerland: Trans Tech Pulications Ltd)
[17] Hong C, Huang X and Winther G 2013 *Phil. Mag.* **93** 3118–3141
[18] Jones A R, Ralph B and Hansen N 1979 *Proc R Soc London A* **368** 345
[19] Liu Q 1995 *Ultramicroscopy* **60** 81-9
[20] Martorano M A, Sandim H R Z, Fortes M A and Padliha A F 2007 *Scripta Mater.* **56** 903-6
[21] Zhang Y B, Godfrey A and Juul Jensen D 2009 *Computers, Materials & Continua* **14** 197-207
[22] Martorano M A, Fortes M A and Padilha A F 2006 *Acta Mater.* **54** 2769-76
[23] Sun J, Zhang Y B, Dahl A B, Conradsen K and Juul Jensen D 2015 *Proc. 36th Risø Int. Symp. on Mater. Sci* (*Roskilde*, *DK*, *2015*), ed S Fæster et al. (Roskilde: Risø)
[24] Juul Jensen D, Lin F X, Zhang Y B and Zhang Y H 2013 *Mater. Sci. Forum* **753** 37-41

[25] Spanos G, Rowenhorst D J, Chan S and Olson G B 2010 *Proc. 31st Risø Int. Symp. on Mater. Sci* (*Roskilde*, *DK*, *2010*), ed N Hansen et al (Roskilde: Risø) pp. 159-70
[26] Uchic M D, Holzer L, Inkson B J, Principe E L and Munroe P 2007 *MRS Bull* **32** 408-16
[27] Zaefferer S, Wright S I and Raabe D 2008 *Metall. Mater. Trans.* **39A** 374-89
[28] Zhang Y, Juul Jensen D, Zhang Y B, Lin F X, Zhang Z and Liu Q. 2012 *Scr. Mater.* **67** 320-3
[29] Rowenhorst D J, Gupta A, Feng C R and Spanos G 2006 *Scr. Mater.* **55** 11-6
[30] Echlin M P, Husseini N S, Nees J A and Pollock T M 2011 *Adv. Mater.* **23** 2339-42
[31] Spowart J E 2006 *Scr. Mater.* **55** 5-10
[32] Fan G H, Zhang Y B, Driver J H and Juul Jensen D 2014 *Scr. Mater.* **72-73** 9-12
[33] Xu W, Quadir M Z and Ferry M 2009 *Metall. Mater. Trans.* **40A** 1547-56
[34] Zhang Y B, Godfrey A, MacDonald N and Juul Jensen D 2012 *Proc. 1st Int. Conf. on 3D Material Science* ed M De Graef et al. (Wiley) pp 31-6
[35] Duggan B J, Lucke K, Kohlhoff G and Lee C S 1993 *Acta Metall. Mater.* **41** 1921
[36] Faivre P and Doherty R D 1979 *J. Mater. Sci.* **14** 879-919
[37] Berger A, Wilbrandt P-J, Ernst F, Klement U and Haasen P 1988 *Prog. Mater. Sci.* **32** 1-95
[38] Zhang Y B, Elbrønd A and Lin F X 2014 *Materials Characterization* **96** 158-65
[39] Zhang Y B, Godfrey A and Juul Jensen D 2013 *Mater. Sci. Forum* **753** 117-20
[40] Zhang Y B, Godfrey A and Juul Jensen D 2010 *Proc. 31st Risø Int. Symp. on Mater. Sci* (*Roskilde*, *DK*, *2010*), ed N Hansen et al. (Roskilde: Risø) pp. 497-503
[41] Lens A, Maurice C and Driver J H 2005 *Mater Sci Eng A* **403** 144-53
[42] Le Gall R, Liao G and Saindrenan G 1999 *Scr. Mater.* **41** 427-32
[43] van der Zwaag S, Anselmino E, Miroux A and Prior D J 2006 *Mater. Sci. Forum* **519-521** 1341-8
[44] Hurley P J and Humphreys F J 2004 *J. Microsc* **213** 225-34
[45] Moelans N, Godfrey A, Zhang Y B and Juul Jensen D 2013 *Phys. Rev. B* **88** 054103
[46] Moelans N, Zhang Y B, Godfrey A and Juul Jensen D 2015 *Proc. 36th Risø Int. Symp. on Mater. Sci* (*Roskilde*, *DK*, *2015*), ed S Fæster et al. (Roskilde: Risø)
[47] Zhang Y B, Godfrey A, Liu Q, Liu W and Juul Jensen D 2009 *Acta Mater.* **57** 2632-39
[48] Zhang Y B, Godfrey A and Juul Jensen D 2014 *Metal. Mater. Trans.* **45A** 2899-905
[49] Juul Jensen D and Poulsen H F 2012 *Materials Characterization* **72** 1–7
[50] Poulsen H F, Ludwig W, Lauridsen E M, Schmidt S, Pantleon W, Olsen U L, Oddershede J, Reischig P, Lyckegård A, Wright J and Vaughan G 2010 *Proc. 31st Risø Int. Symp. on Mater. Sci* (*Roskilde*, *DK*, *2010*), ed N Hansen et al. (Roskilde: Risø) pp. 101-120
[51] Larson B, Yang W, Ice G, Budai J and Tischler J 2002 *Nature* **415** 887–890
[52] Simons H, King A, Ludwig W, Detlefs C, Pantleon W, Schmidt S, Snigireva I, Snigirev A and Poulsen H F 2014 *Nature Communications* **6** 6098
[53] Ice G E, Pang J W L, Barabash R I and Puzyrev Y 2006 *Scr. Mater.* **55** 57-62
[54] Pang J W L, Ice G E and Liu W 2010 *Mater. Sci. Eng.* **528** 28-31
[55] van Boxel S, Schimdt S, Ludwig W, Zhang Y B, Juul Jensen D and Pantleon W 2014 *Materials Transactions* **55** 128–136
[56] Ahl S R, Simons H, Jakobsen A C, Zhang Y B, Juul Jensen D and Poulsen H F 2015 *Proc. 36th Risø Int. Symp. on Mater. Sci* (*Roskilde*, *DK*, *201*), ed S Fæster et al. (Roskilde: Risø)
[57] http://imagej.nih.gov/ij/index.html
[58] Groeber M A and Jackson M A 2014 *Intergrating Materials and Manufacturing Innovation.* **3** 5
[59] Bachmann F, Hielscher R and Schaeben H 2010 *Solid State Phenomena* **160** 63-8
[60] Gottstein G and Shvindlerman L S 1992 *Scripta Metall. Mater.* **27** 1521-6
[61] http://www.j-tec.co.jp/english/focusing/index.html
[62] Olmsted D L, Holm E A and Foiles S M 2009 *Acta Mater.* **57** 3704-13
[63] Homer E 2015 *Proc. 36th Risø Int. Symp. on Mater. Sci* (*Roskilde*, *DK*, *2015*), ed S Fæster et al. (Roskilde: Risø)